Molecular recognition of a single sphingolipid species by a protein's transmembrane domain

F.-Xabier Contreras*[1], Andreas M. Ernst*[1], Per Haberkant[2], Patrik Björkholm[3,4], Erik Lindahl[3,5], Başak Gönen[1], Christian Tischer[6], Arne Elofsson[3,4], Gunnar von Heijne[3,4], Christoph Thiele[7], Rainer Pepperkok[6], Felix Wieland[1#], and Britta Brügger[1#]

[1]Heidelberg University Biochemistry Center, Im Neuenheimer Feld 328, 69120 Heidelberg, Germany

[2]present address: Cell Biology and Biophysics Unit EMBL, Meyerhofstrasse 1, 69117 Heidelberg, Germany

[3]Center for Biomembrane Research, Department of Biochemistry and Biophysics, Stockholm University, SE-106 91 Stockholm, Sweden

[4]Stockholm Bioinformatics Center, Science for Life Laboratory Stockholm University, Box 1031, SE-171 21 Solna, Sweden

[5]Theoretical & Computational Biophysics, Royal Institute of Technology, AlbaNova University Centre, SE-106 91 Stockholm, Sweden

[6]ALMF, EMBL, Meyerhofstrasse 1, 69117 Heidelberg, Germany

[7]LIMES Life and Medical Sciences Institute, Carl-Troll-Str. 31, 53115 Bonn, Germany

[*]these authors contributed equally to this work

[#]corresponding authors

Functioning and processing of membrane proteins critically depend on the way their transmembrane segments are embedded in the membrane[1]. Sphingolipids are structural components of membranes and can also act as intracellular second messengers. Not much is known of sphingolipids binding to transmembrane domains (TMDs) of proteins within the hydrophobic bilayer, and how this could affect protein function. Here we show a direct and highly specific interaction of exclusively one sphingomyelin species, SM 18, with the TMD of the COPI machinery protein p24[2]. Strikingly, the interaction depends on both the headgroup and the backbone of the sphingolipid, and on a signature sequence (VXXTLXXIY) within the TMD. Molecular dynamics simulations show a close interaction of SM 18 with the TMD. We suggest a role of SM 18 in regulating the equilibrium between an inactive monomeric and an active oligomeric state of the p24 protein[3,4], which in turn regulates COPI-dependent transport. Bioinformatic analyses predict that the signature sequence represents a conserved sphingolipid-binding cavity in a variety of mammalian membrane proteins. Thus, in addition to a function as second messengers, sphingolipids can act as cofactors to regulate the function of transmembrane proteins. Our discovery of an unprecedented specificity of interaction of a TMD with an individual sphingolipid species adds to our understanding why biological membranes are assembled from such a large variety of different lipids.

Lipidomics of Golgi-derived COPI vesicles unravelled a partial segregation of cholesterol and most SM species except for one (N-stearoyl SM) from the vesicle fraction[5]. In order to understand the molecular mechanisms of SM 18 enrichment in vesicles, we investigated *in vivo* binding of lipids to p24 and p23, membrane proteins involved in COPI vesicle biogenesis (Supplementary Fig. 1)[6]. Lipid crosslinking[7,8] revealed a strong sphingolipid labelling of p24 (Fig. 1a-b, see also Supplementary Fig. 2), with a 5-fold higher recovery of radioactivity/mol protein compared to p23. In order to analyse if this interaction of p24 with SM is specific for SM 18, we established a liposomal assay to study TMD-lipid interactions (see Supplementary Fig. 3). MBP fusions of the TMDs of p23 and p24 were analysed in a liposomal FRET system for their interaction with pentaenoyl-SM 18 (SM 18:5, as a fluorescently labelled analogue of endogeneous SM 18:O[9], see Supplementary Information), pentaenoyl-ceramide (Cer) 18, or pentaenoyl-PC 18 (Fig. 1c). Distinct FRET was observed between the TMD of p24 and SM 18:5, but not with the TMD of p23. A mutant lacking the single Trp residue within the TMD (p24(TMD)W4A) did not trigger a FRET. With ceramide 18:5 no FRET was observed for any TMD. With PC 18:5 weak FRET was observed with the p24(TMD), and a slightly stronger signal was obtained with p23(TMD). Together these results show a marked specificity of p24 for SM, with both the hydrophobic moiety and the hydrophilic choline phosphate headgroup needed for the interaction. We next analysed the extent of FRET obtained between the TMDs of p24 and p23 and pentaenoyl-SMs covering the range of the major endogenous molecular species from C14 to C24. A remarkable specificity was observed for the interaction of p24 with SM 18 in liposomes composed of DOPC:PE:pentaenoyl-SM (Fig. 1d, left panel). In liposomes more closely reflecting the

lipid composition of the mammalian Golgi apparatus we again observed a striking specificity observed for SM 18, with weak but significant signals for SM 20 and SM 22 (Fig. 1d, right panel). In contrast, the TMD of p23 did not give rise to comparable FRET with any of the SM species.

In order to define the structural prerequisites for SM 18 binding, we performed an Ala scan across the TMD of p24 starting with position 8 within the TMD, leaving three amino acids before and after W4 unchanged, in order to minimise a direct influence on the biophysical properties of the FRET donor. Two groups of mutants were observed, with a strong inhibition of FRET with Ala substitutions in positions 8, 10, 11, 12, 15, 19 and 20 (group 1), and less inhibition in positions 13, 16, 17, 18, and 21 (group 2) (Supplementary Fig. 4). Although group 1 mutants showed a strong inhibition of FRET, they maintained a high degree of specificity for SM 18:5 (e.g. V11A, Supplementary Fig. 5a). In contrast, group 2 mutants V13, T16, L17, and Y21 displayed strongly compromised species specificity (Supplementary Fig. 5c-f). Mutant G18A was not further investigated, because G18W had not revealed an alteration of SM 18 binding (Supplementary Fig. 3d), suggesting that G18 is not directly involved in the lipid-p24 interaction. From the above data we reckoned that a C-terminal motif made of amino acid residues V13, T16, L17, and Y21 of the p24 TMD (V181, T184, L185, and Y189 in the full-length protein) represents a structural determinant for the specific binding of SM 18 (see also Supplementary Discussion). An energy-minimised projection of the TMD yielded the structure depicted in Fig. 2a (left). In this model, a groove is formed from the Tyr residue in position 21 to the Val residue in position 13. Within the SM-binding motif, the β-branched residue Ile is found in position 20 of the TMD. ß-branched residues were

shown to contribute to TMD-TMD interactions[10,11] by conveying higher rigidity and thereby allowing for stronger London dispersion forces. In the model, this residue is part of the cavity and thus is likely to contribute to the binding motif. If this groove indeed accommodates the backbone of SM 18, the insertion of a bulky hydrophobic residue in position 17 should prevent lipid binding. In order to fill this cavity with minimal alterations of the helical structure[12] we introduced a Phe residue in position 17 of the TMD. FRET analysis revealed that binding of SM 18 was completely inhibited (Fig. 2b). In order to challenge the existence of a C-terminal binding motif, we transferred the C-terminal half of the p24 TMD to the N-terminal half of the non-SM-binding TMD of p23. The chimeric TMD yielded 50% of the level of FRET as compared to the TMD of p24 (Fig. 2b). Interestingly, the chimera shows promiscuity with regard to the SM molecular species, binding significant amounts of SM 20 and SM 22 in addition to SM 18 (Supplementary Fig. 5b), pointing at a contribution of the N-terminal residues to the orientation of the SM-binding pocket. The loss of FRET by mutant p24(TMD)L17F suggested a loss of SM 18 binding. To test loss of binding *in vivo*, full-length p24 wt and p24L17F were expressed as YFP fusion proteins (Supplementary Fig. 6a). Sphingolipid labelling showed that p24L17F has lost the capability to bind SM *in vivo* (Fig. 2c). SM is known to be synthesised in the luminal leaflet, however, *in vitro* experiments suggest that sphingolipids can flip between the two leaflets stimulated by free ceramide that translocates from the cytoplasmic to the luminal leaflet of membranes[13] (see also Supplementary Fig. 6b). In addition, *in vivo* analyses employing the SM-binding toxin Equinatoxin II point to an occurrence of SM in the cytoplasmic leaflet of the Golgi membrane [14].

In order to understand binding selectivity at the molecular level, we compared the structural features of SM molecular species (see Supplementary Fig. 7). MD simulations and monolayer experiments[15-17] suggest that only the SM species with a suitable dynamic volume would fit into the cavity of the p24 TMD formed by V13, T16, and L17, excluding lipids with larger dynamic volume (SM 14 and 16, see Supplementary Fig. 7). SM species with smaller dynamic volumes, however, would need to be excluded from the hydrophobic cavity by a different mechanism (see Supplementary Discussion).

We next investigated the binding signature through a series of five molecular simulations of the TMD of p24 embedded in a POPC bilayer including SMs with fatty acids of C14 to C22. By extending all atomistic simulations to 1 μs we observe spontaneous diffusion of SMs to the TMD and close interaction with the proposed binding site primarily for SM 18, and to a minor extend also SM 16 and SM 20 (Supplementary Fig. 8). The polar head group of SM 'wraps around' the Y21 side chain, while the C18 chain continues down around the helix and packs in the groove between V13/T16/L17 (Fig. 2d, and Supplementary movie 1). The sphingosine chain packs in the groove below V13. The other SM molecular species also approach the p24 TMD, but steric effects appear to make interactions more difficult in these cases. For instance, the SM 14 lipid head group rather interacts with Y21 by packing mostly below the side chain, which rotates both lipid chains away from the helix and prevents efficient packing (Supplementary movie 2). The lifetime of the SM 18-p24 (TMD) complex in the molecular dynamics simulation was of the order of 250 ns, which is 5 times longer than observed for the other SM species. Likewise, as compared to SM 18, the relative dissociation constant of SM 14 was 6.5-fold higher (Supplementary Fig. 9). Notably, although the TMD of p24 is highly

conserved in higher eukaryotes, it is not conserved in yeast, in agreement with the absence of SM in this organism.

In order to search for other candidate sphingolipid-interacting proteins, we defined a binding signature where either a β-branched residue (I, T, V) or Leu is allowed in any of the first four positions, and an aromatic residue (F, W, Y) is allowed in the last position (Fig. 3a). The signature represents $4^4 \cdot 3 = 768$ unique sequence motifs, 13 of which were found to be overrepresented in a set of mammalian membrane proteins (see Full Methods). These 13 motifs identified 48 candidate proteins (Supplementary Table 1), mostly localised to the plasma membrane (Fig. 3b).

Three recombinant candidates and, as a negative control, the non-signature containing asialo-glycoprotein receptor, were expressed in HeLa cells (Supplementary Fig. 10). In *in vivo* labelling all three candidates showed strong binding to a sphingolipid (Fig. 3c). Interestingly, INGR1 binds to a sphingolipid only upon activation by its ligand interferon γ.

What may be the function of the highly specific interaction of SM 18 with p24? As p24 acts as membrane machinery for the formation of COPI vesicles, we analysed if a loss of binding of SM 18 would affect transport of biosynthetic cargo[18,19]. We analysed transport of vesicular stomatitis G (VSV-G) protein[20,21] to determine the transport rates in HeLa cells stably transfected with full-length p24 wt or p24L17F, N-terminally fused to YFP. Expression of p24L17F caused an acceleration of VSV-G protein transport (Fig. 4a), resulting in a 2.5fold increase of the fraction of total VSV-G that reached the plasma membrane at t = 45 min (see also Supplementary Fig. 11a-b).

How can a marked acceleration of transport be caused by a lack of binding of SM 18 to p24? A decrease in recycling efficiency would cause an increased anterograde transport of this cargo, and should affect Golgi export. To test this possibility, we measured Golgi export kinetics employing fluorescence loss in photobleaching (FLIP). While Golgi-associated fluorescence of YFP-p24 wt was reduced to 50% within 4.5 min, the half-life of Golgi residence of YFP-p24L17F was significantly prolonged to 7 min (Fig. 4b, for controls see Supplementary Fig. 11c). To analyse if indeed retrograde transport from the Golgi to the ER is affected we monitored trafficking to the ER of *Pseudomonas aeroginosa* exotoxin A (PE-A). The toxin is transported from the Golgi to the ER in a COPI-dependent manner[22]. In contrast to cells expressing YFP-p24, YFP-p24L17F-cells showed a significant reduction of PE-A-dependent inhibition of protein biosynthesis, the readout for exotoxin transport to the ER (Fig. 4c, for controls see Supplementary Fig. 11d) Together, these data imply that efficient retrograde COPI-dependent transport depends on binding of p24 to SM.

To test if binding to SM 18 might help organise the dimeric, transport active state of p24, by affecting its monomer/oligomer equilibrium via the TMD, we employed a chemical crosslinking assay with proteoliposomes reconstituted from p24 family-TMD fusion proteins and SMs of various species compositions. Indeed, dimerisation is significantly induced only in liposomes containing both SM 18 and p24 (Fig. 4d, and Supplementary Fig. 12a-c). To analyse if dimerisation of p24 is also affected *in vivo* in the presence of full-length p24L17F, we monitored dimerisation of p24 employing an *in situ* protein-protein interaction assay. Signals were significantly reduced in the presence of p24L17F (Fig. 4e, for representative images and Western blots see Supplementary Fig. 12d).

Similar results were obtained when cells expressing either YFP-p24 wt or YFP-p24L17F were subjected to chemical crosslinking (Supplementary Fig. 12e).

How might a complex of dimeric p24 and SM 18 be organised? We performed molecular dynamics simulations starting from different models based on the SM-bound monomeric structures from the initial simulations. The most stable model was one with a rather polar dimerisation interface not overlapping with the SM binding site (Fig. 4f); this complex remained intact for at least 200 ns. Besides a direct role of SM in stabilising a p24 dimer, other mechanisms of SM-triggered dimerisation might apply, such as a SM-dependent conformational change of p24 or build-up of high concentrations of p24 in SM 18 microdomains.

In summary, we have uncovered an unprecedented specificity of interaction between an individual sphingolipid species and a TMD, and have defined a structural signature within the TMD for this binding. Specific binding of individual lipid species to TMDs of membrane proteins may serve different functions and help to understand the need for the complexity of membrane lipid compositions at a functional level.

Methods Summary

In vivo photoaffinity labelling of CHO cells.

Cells were labelled with the different photoactivatable precursors as described[7,8]. Briefly, cells were washed with PBS, followed by addition of freshly prepared delipidated medium containing lipid precursors. After labelling, the medium was removed and cells were washed twice with PBS. After UV-irradiation, cells were harvested and lysed in lysis buffer [50 mM HEPES-NaOH, pH 7.4, 100 mM NaCl, 5 mM EDTA, 1% Triton X-100 (v/v), 0.5% deoxycholate (w/v), and protease inhibitor cocktail]. After lysis, samples were subjected to immunoprecipitation. Following SDS-PAGE and Western blotting, radioactively labelled proteins were detected by digital autoradiography (β-Imager 2000, Biospace).

FRET assay. Förster resonance energy transfer (FRET) was used to directly probe the interaction of TMDs with pentaenoyl-lipids. FRET experiments were conducted on a Jasco 6500 unit spectrofluorometer (Jasco). Proteoliposomes (protein/lipid, 1:5000) were diluted in a quartz cuvette in buffer (10 mM HEPES/KOH pH 7.4) to a final concentration of 0.1 mM. The proteoliposomes were incubated at 25°C for 5 min under continuous stirring. The extent of FRET between TMD and pentaenoyl-lipids was determined recording emission spectra from 310-540 nm. Emission spectra were collected, exciting at 280 nm the Trp present in the TMD. Slit widths of 5 nm were used for both excitation and emission.

Full Methods and any associated references are available as Supplementary information.

References

1 Coskun, U. & Simons, K. Cell membranes: the lipid perspective. *Structure* **19**, 1543-1548 (2011).

2 Popoff, V., Adolf, F., Brugger, B. & Wieland, F. COPI Budding within the Golgi Stack. *Cold Spring Harb Perspect Biol* **3** (2011).

3 Bethune, J. *et al*. Coatomer, the coat protein of COPI transport vesicles, discriminates endoplasmic reticulum residents from p24 proteins. *Mol Cell Biol* **26**, 8011-8021 (2006).

4 Reinhard, C. *et al*. Receptor-induced polymerization of coatomer. *Proc Natl Acad Sci U S A* **96**, 1224-1228 (1999).

5 Brügger, B. *et al*. Evidence for segregation of sphingomyelin and cholesterol during formation of COPI-coated vesicles. *J Cell Biol* **151**, 507-518 (2000).

6 Beck, R., Ravet, M., Wieland, F. T. & Cassel, D. The COPI system: molecular mechanisms and function. *FEBS Lett* **583**, 2701-2709 (2009).

7 Haberkant, P. *et al*. Protein-sphingolipid interactions within cellular membranes. *J Lipid Res* **49**, 251-262 (2008).

8 Thiele, C., Hannah, M. J., Fahrenholz, F. & Huttner, W. B. Cholesterol binds to synaptophysin and is required for biogenesis of synaptic vesicles. *Nat Cell Biol* **2**, 42-49 (2000).

9 Kuerschner, L. *et al*. Polyene-lipids: a new tool to image lipids. *Nat Methods* **2**, 39-45 (2005).

10 Russ, W. P. & Engelman, D. M. The GxxxG motif: a framework for transmembrane helix-helix association. *J Mol Biol* **296**, 911-919 (2000).

11 Senes, A., Gerstein, M. & Engelman, D. M. Statistical analysis of amino acid patterns in transmembrane helices: the GxxxG motif occurs frequently and in association with beta-branched residues at neighboring positions. *J Mol Biol* **296**, 921-936 (2000).

12 Jones, D. T., Taylor, W. R. & Thornton, J. M. A mutation data matrix for transmembrane proteins. *FEBS Lett* **339**, 269-275 (1994).

13 Contreras, F. X., Basanez, G., Alonso, A., Herrmann, A. & Goni, F. M. Asymmetric addition of ceramides but not dihydroceramides promotes transbilayer (flip-flop) lipid motion in membranes. *Biophys J* **88**, 348-359 (2005).

14 Bakrac, B. *et al*. A toxin-based probe reveals cytoplasmic exposure of Golgi sphingomyelin. *J Biol Chem* **285**, 22186-22195.

15 Li, X. M., Smaby, J. M., Momsen, M. M., Brockman, H. L. & Brown, R. E. Sphingomyelin interfacial behavior: the impact of changing acyl chain composition. *Biophys J* **78**, 1921-1931 (2000).

16 Niemela, P., Hyvonen, M. T. & Vattulainen, I. Structure and dynamics of sphingomyelin bilayer: insight gained through systematic comparison to phosphatidylcholine. *Biophys J* **87**, 2976-2989 (2004).

17 Niemela, P. S., Hyvonen, M. T. & Vattulainen, I. Influence of chain length and unsaturation on sphingomyelin bilayers. *Biophys J* **90**, 851-863 (2006).

18 Presley, J. F. *et al*. ER-to-Golgi transport visualized in living cells. *Nature* **389**, 81-85 (1997).

19 Scales, S. J., Pepperkok, R. & Kreis, T. E. Visualization of ER-to-Golgi transport in living cells reveals a sequential mode of action for COPII and COPI. *Cell* **90**, 1137-1148 (1997).
20 Keller, P., Toomre, D., Diaz, E., White, J. & Simons, K. Multicolour imaging of post-Golgi sorting and trafficking in live cells. *Nat Cell Biol* **3**, 140-149 (2001).
21 Simpson, J. C. *et al*. An RNAi screening platform to identify secretion machinery in mammalian cells. *J Biotechnol* **129**, 352-365 (2007).
22 Jackson, M. E. *et al*. The KDEL retrieval system is exploited by Pseudomonas exotoxin A, but not by Shiga-like toxin-1, during retrograde transport from the Golgi complex to the endoplasmic reticulum. *J Cell Sci* **112 (Pt 4)**, 467-475 (1999).

Supplementary Information is linked to this manuscript.

Acknowledgments

The authors would like to thank Timo Sachsenheimer for technical assistance, Alexander Brodde for help with lipid synthesis, Dan Cassel for comments on the manuscript, and the members of the Wieland lab for discussion. This work was supported by a grant of the German research foundation (DFG, TRR83) to B.B. and F.W. and by an ERC grant (209825) to E.L. F.X.C. was supported by a FEBS fellowship and A.M.E. by the Peter and Traudl Engelhorn foundation.

Author Contributions

F.X.C., A.M.E., and P.H. designed and performed the experiments. P.B. performed the bioinformatics analyses under the supervision of A.E., G.v.H., and A.M.E. E.L. designed, performed and interpreted MDS experiments. B.G. performed *in vivo* crosslinking experiments. C.Th. provided reagents and helped to establish photolabelling and FRET experiments. C.Ti. and R.P. provided reagents and tools and supported A.M.E.

concerning VSV-G experiments. F.W. and B.B. designed the experiments and wrote the manuscript.

Author Information

The authors declare no competing financial interests. Correspondence and requests for material should be addressed to F.W. and B.B. (felix.wieland@bzh.uni-heidelberg.de, britta.bruegger@bzh.uni-heidelberg.de).

Figure Legends

Fig. 1 p24 specifically interacts with SM 18. **a**, CHO cells were grown in the presence of 200 μCi of [^{3}H]-photoSph. Cells were UV-irradiated, lysed and subjected to immunoprecipitation using antibodies against p23 or p24. Radioactivity recovered of input, supernatant (SN) and immunoprecipitation (IP) was visualised by autoradiography (upper panels). Lower panels, Western blot analysis. **b**, Quantitation of immunoprecipitated radioactivity. **c**, *In vitro* FRET analysis of MBP-TMD fusion proteins and pentaenoyl-lipids. Proteoliposomes contained either SM 18:5, Cer 18:5, or PC 18:5. Red curve, p23(TMD); black curve, p24(TMD); blue curve, p24(TMD)W4A. **d**, Proteoliposomes were prepared in the presence of p24(TMD) (black bars) or p23(TMD) (grey bars) and 1 mol% of pentaenoyl-SMs, mimicking a liquid-disordered phase (left panel) or a mammalian Golgi membrane (right panel). Data are normalised to background-subtracted fluorescence of SM 18:5, and are the mean ± SD of three experiments.

Fig. 2 Characterisation of the SM-binding pocket. **a**, Energy-minimised structure of p24(TMD), p23(TMD), p24(TMD)L17F, and p24/p23 chimeric TMD. Residues of p24 involved in SM 18 recognition are depicted in red, the L17F mutation is highlighted in green. **b,** Proteoliposomes containing p24(TMD), p23(TMD), p24(TMD)L17F or the p24/p24-TMD chimera were prepared in the presence of 1 mol% of pentaenoyl-SM (18:5) (DOPC/PE/pentaenoyl-SM, molar ratio 89/10/1). FRET measurements were performed as decribed above. Data are the mean ± S.D. of three independent experiments. **c**, *In vivo* binding of [^{3}H]-sphingolipids to YFP-p24 wt and YFP-p24L17F. Upper panel, autoradiography; lower panel, Western blot. **d**, Molecular dynamics simulations: snapshot of a SM 18-p24(TMD) interaction. The interacting lipid and residues displaying the signature are highlighted. Blue, p24(TMD); red, SM-binding pocket, yellow; SM 18:0 head group; green, SM 18:0 backbone and N-acylated fatty acid.

Fig. 3 A conserved sphingolipid binding signature. **a,** Signature patterns used for both randomisation/shuffling approach and screening for potential sphingolipid-binding proteins (upper panel). All possible combinations were analysed for significant overrepresentations in TMDs. Motifs overrepresented with a p-value ≤ 0.05 were used to generate the sequence logo (lower panel). The letter size corresponds to the probability to find this amino acid at that position. Each dot below the line represents an amino acid position. **b**, Intracellular distribution of signature-containing transmembrane protein candidates. **c**, *In vivo* labelling of flag-tagged constructs of INGR1_HUMAN, I17RB_HUMAN, B3GT2_HUMAN, and ASGR1_HUMAN. Cells were labelled with

[^{3}H]-photo-sphingosine, UV-irradiated, lysed and subjected to IP using an antibody against the flag tag (α-F). Radioactivity recovered with protein candidates was visualised by autoradiography. The corresponding proteins were detected by Western blot analysis. Asterix, expected size of proteins.

Fig. 4 Binding of SM 18 to p24(TMD) affects protein transport and triggers p24 dimerisation. **a**, Expression of p24L17F accelerates transport of ts-O45-G protein. For each time point and experiment (n=3), at least 600 cells were analysed. **b**, Comparison of the average half lives of decay in fluorescence in Golgi of YFP-p24 and YFP-p24L17F. Data represent the mean of n = 22-24 experiments ± SE. p-value of two-tailed, unpaired t-test < 0.0001 (***) is given. **c**, Expression of YFP-p24L17F reduces toxicity of PE-A. Error bars, SEM. Statistics: two-tailed, unpaired t-test. **d**, SM 18:0 induces dimerisation of p24(TMD) (white bars) but not of p23(TMD) (black bars). TMDs reconstituted into proteoliposomes with indicated SM species subjected to chemical crosslinking (n = 4). Results of paired, two-tailed t-tests are given. **e**, Quantification of homodimers in CHO cells *in situ*. Error bars, SEM. Statistics: two-tailed, unpaired t-test. ***, $p < 0.001$ **f**, Model of p24(TMD) SM 18 complexes. Left, side view; right, top view.

Brügger_Figure 1

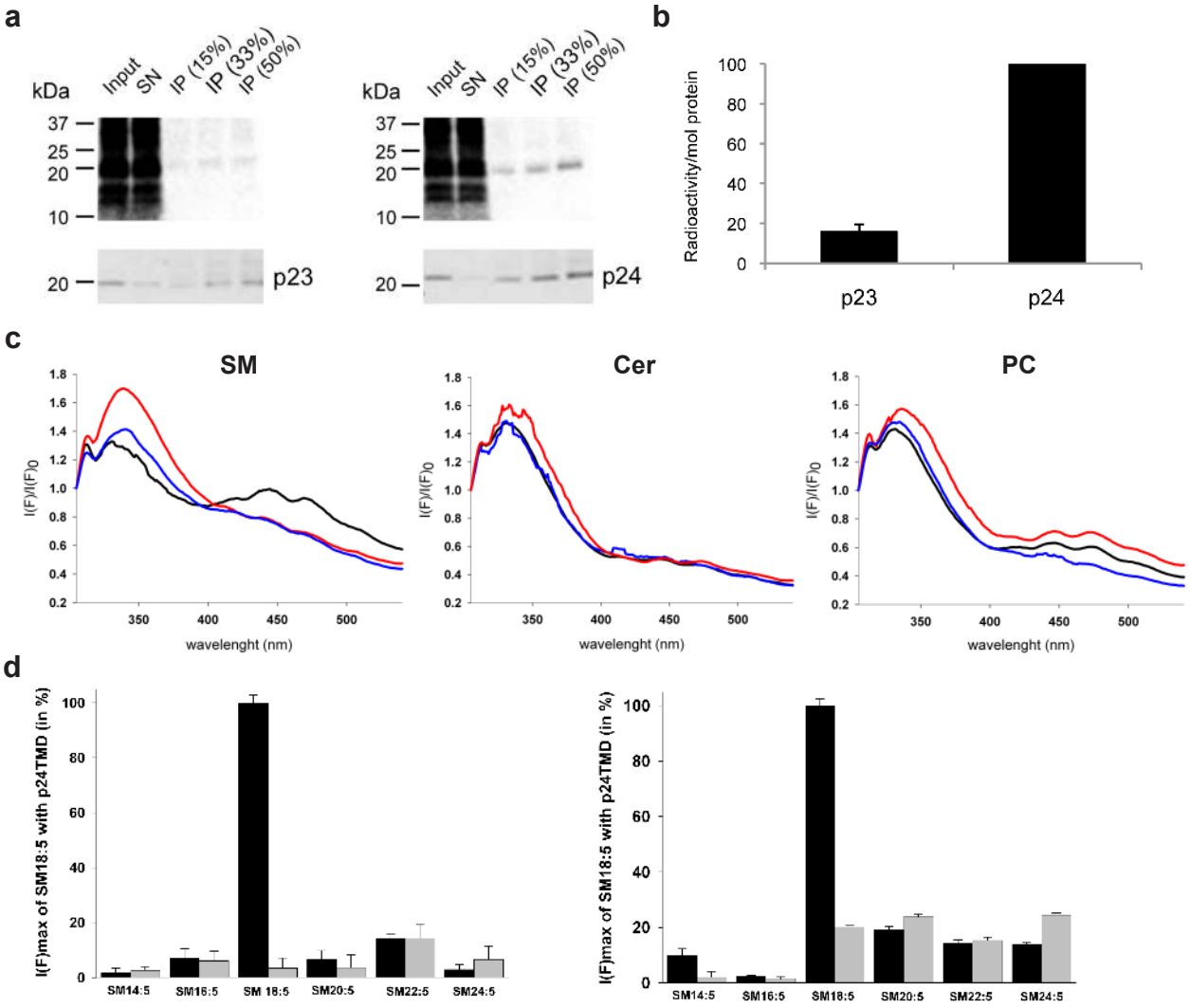

Brügger_Figure 2

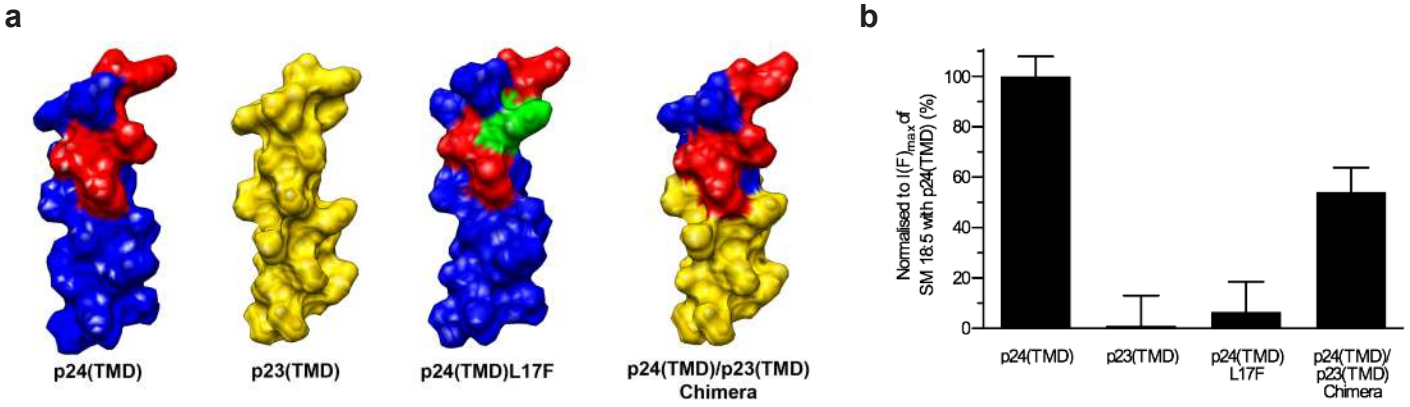

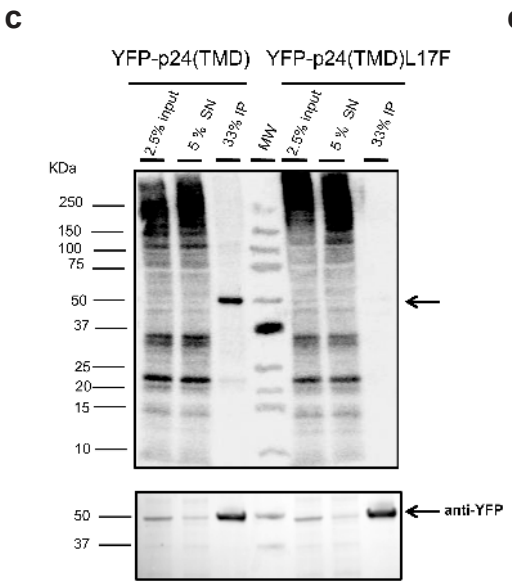

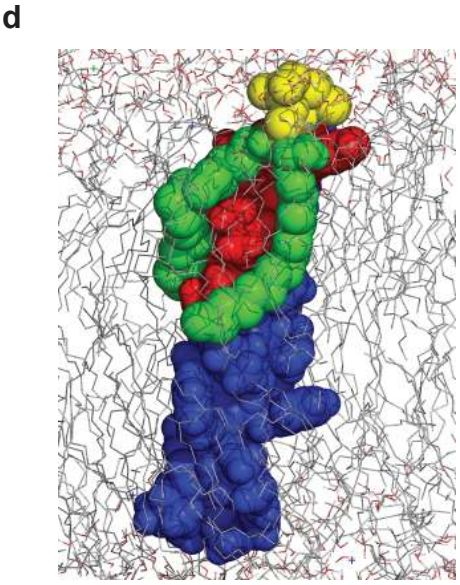

Brügger_Figure 3

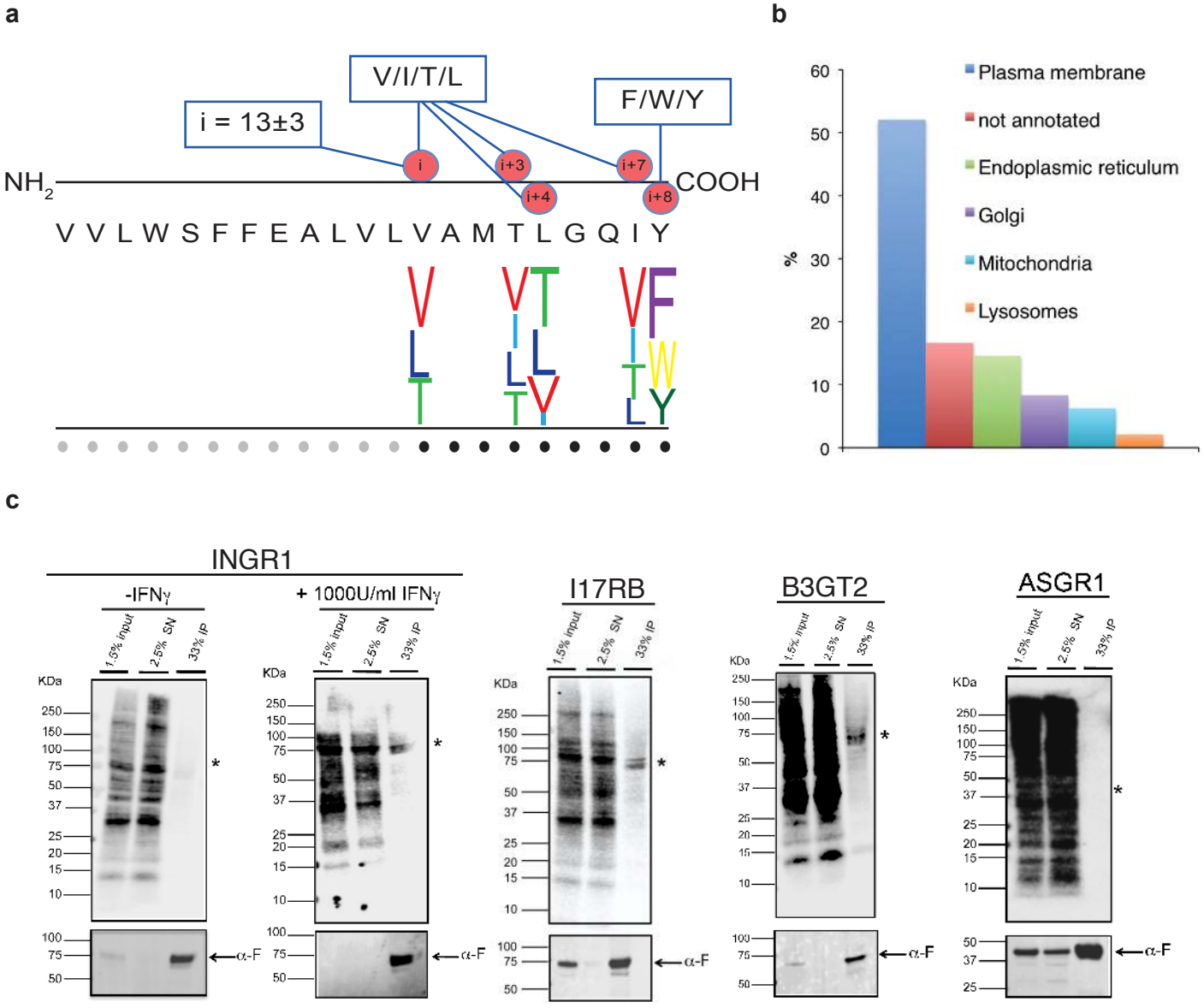

Brügger_Figure 4

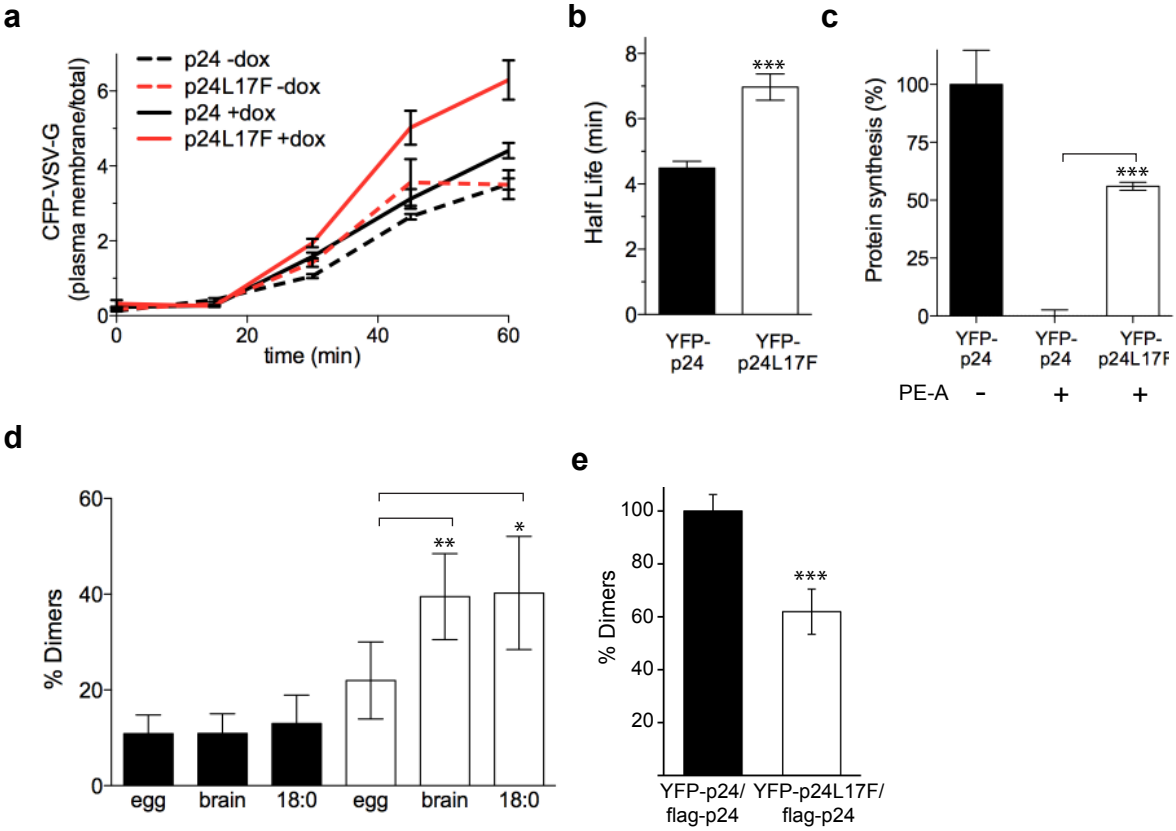

f